



Cite this: *Analyst*, 2020, **145**, 2639

Paper spray mass spectrometry for the analysis of picoliter droplets†

Ravleen Kaur Kohli and James F. Davies *

Recent experimental efforts have shown that single particle levitation methods may be effectively coupled with mass spectrometry (MS) using paper spray (PS) ionization for compositional analysis of picoliter droplets. In this work, we characterize the response of PS–MS to analytes delivered in the form of picoliter droplets and explore its potential for identification and quantification of these samples. Using a microdroplet dispenser to generate droplets, we demonstrate sensitivity to a range of oxygenated organic molecules typical of compounds found in atmospheric secondary organic aerosol. We assess experimental factors that influence the reproducibility and sensitivity of the method and explore the linearity of the system response to increasing analyte mass in droplets containing single or multicomponent analytes. We show that the ratio of analyte signal from multicomponent samples may be used to characterize the relative composition of the system. These measurements demonstrate that the droplet PS–MS method is an effective tool for qualitative and quantitative analysis of single picoliter droplets containing picogram levels of analyte. The potential applications of this technique for characterizing the composition of levitated particles will be discussed.

Received 13th December 2019,

Accepted 10th February 2020

DOI: 10.1039/c9an02534k

rsc.li/analyst

1. Introduction

Aerosol particles‡ are a major component of the atmosphere and affect the formation, lifetime and optical properties of clouds,^{1–3} absorb and scatter incoming solar radiation,^{4,5} provide surfaces on which chemistry can occur,^{6–8} and negatively influence air quality and health.^{9,10} Their composition spans a broad range of compounds and due to the oxidizing conditions in the atmosphere their composition is continuously evolving.^{11,12} The composition of aerosol particles play a defining role in regulating their impacts in the atmosphere. Efforts to measure the composition of aerosol have relied on mass spectrometry, and the aerosol mass spectrometer (AMS) has been used extensively.^{13–15} The AMS has been used in both field campaigns and laboratory measurements and works by directly sampling an aerosol *via* flash vaporization and electron-impact ionization to provide composition information.¹⁶ Soft ionization methods have also been used to gain more insight into aerosol samples, such as chemical ionization (CI),^{17,18} plasma-based methods such as direct analysis in real-time (DART) ionization^{19–21} and flowing atmospheric-pressure

afterglow ionization,²² droplet-assisted inlet ionization,²³ and photoionization.²⁴ These ionization methods yield more detailed molecular information, improving our knowledge of the composition of atmospheric aerosol. Composition alone, however, is not enough to classify and understand the impacts of aerosol in the atmosphere and we must couple knowledge of particle composition with their physical and optical properties and chemical reactivity.²⁵

Single particle levitation methods have been developed over many years as effective tools for probing the physical and optical properties of micron-sized samples.²⁶ The application of these methods to probing the dynamics of atmospheric aerosol and their proxies have revealed important information relating to the hygroscopicity, volatility, optical properties, viscosity, surface tension and diffusive characteristics.^{27–36} Although functional group information is available through the use of Raman scattering,³⁴ these methods are typically blind to the exact composition of the sample and instead rely on indirect indicators of composition (size, refractive index *etc.*). Droplet-based ionization methods, such as field-induced droplet ionization (FIDI), laser desorption ionization and droplet electrospray ionization, have been applied to droplet trains and acoustically levitated droplets.^{37–39} However, there is a growing effort to develop experimental platforms capable of measuring the composition of much smaller levitated particles held in electrodynamic traps, and recent work by Jacobs *et al.*⁴⁰ and Birdsall *et al.*^{41,42} have demonstrated the coupling of these methods with mass spectrometry.

Department of Chemistry, University of California, Riverside, California 92521, USA.

E-mail: jfdavies@ucr.edu

‡The term ‘particle’ is used generally to refer to either solid particles or liquid droplets. The term ‘droplet’ is used specifically in the case of liquid droplets.

†Electronic supplementary information (ESI) available. See DOI: 10.1039/c9an02534k

In the works of Birdsall *et al.*,⁴¹ a double-ring electrodynamic balance was used to levitate populations of particles that were then deposited, vaporized and ionized in a corona discharge to be sampled by MS. At the same time, Jacobs *et al.*⁴⁰ reported similar levitation methodology using a linear-quadrupole electrodynamic balance (LQ-EDB) and a paper spray (PS) ionization source. These techniques demonstrated that qualitative information on the composition of 20–50 μm sized droplets could be obtained, however the quantitative nature of the methods remains unclear. In more recent work, Birdsall *et al.*⁴² show that vapor pressures may be elucidated from evaporating multi-component droplets, and measurements revealed the role of inorganic salts on the vapor partitioning of the organic compound 2-butenedial. However, the uncertainties reported in their approach limit the accuracy to which thermochemical data may be quantified. To measure chemical kinetics, the sensitivity and precision of the instrument must be sufficient to detect the formation of products, and the response of the system must be well characterized in order to account for the effects of ionization efficiency and non-linearity of signal. As yet, no single particle MS method has demonstrated effective quantitation for chemical kinetic analysis.

The paper spray ionization used by Jacobs *et al.*⁴³ is based on a relatively new method used in analytical chemistry. Paper spray was introduced by R. Graham Cooks and co-workers as a tool for quick and simple sampling of material.^{44,45} Initially conceived as a disposable sampling platform, recent work has shown that a continuous solvent flow may be applied for longer sampling periods.⁴⁶ The ionization mechanism is similar to that of classical electrospray ionization (ESI) where charged droplets are emitted in a spray, rapidly lose solvent to evaporation and fission due to the Rayleigh charge instability. This produces gas phase ions and clusters that are sampled by the MS. The facets that determine the effectiveness of ESI, such as the composition of the solvent and size distribution of droplets in the spray, may also influence the effectiveness of PS.^{47,48} The PS ionization platform can be effectively applied to droplet measurements due to the ease of transfer of a droplet from a LQ-EDB onto the paper substrate. Despite the simplicity of this ionization method, it offers many advantages, such as a constant background measurement between droplet samples and sensitivity to sub-picogram amounts of analyte.⁴⁹

In order to make effective use of the paper spray method for the analysis of picolitre droplets held in our newly developed LQ-EDB platform,⁵⁰ a characterization of its sensitivity and quantitative ability is necessary. In this work, we explore the basic response of paper spray ionization to sampling material contained within picolitre droplets. We demonstrate a range of compounds that may be detected using this technique and establish the conditions and experimental practices required to ensure the data can be interpreted quantitatively. We report the limit of quantification for a model oxygenated organic compound (citric acid) and the limit of linearity for both single and multi-component systems. We conclude by

discussing the applications and limitations of the technique when applied to sample droplets from the LQ-EDB.

2. Experimental

2.1 Sample preparation

The chemicals used in this study were purchased and used without further purification. Quantitative measurements were performed using citric acid (Sigma-Aldrich, USA; $\geq 99.5\%$ purity) and maleic acid (Sigma-Aldrich, USA; $\geq 99\%$ purity) prepared in aqueous solution using purified water (Fisher Chemical, USA; Submicron Filtered). Various polyethylene glycols, dicarboxylic acids and fatty acids (Sigma-Aldrich, USA) were also measured and used as supplied. Solutions of single and mixed solutes were prepared at known concentrations (ranging from 0.01 to 20 g L^{-1}) and transferred to a microdroplet dispenser (Microfab MJ-ABP-01 w/30 μm orifice) to generate picoliter droplet samples. The droplet dispenser was powered by an in-house constructed pulse generator controlled by a DAQ card and LabVIEW software, delivering 20–50 μs pulses with a voltage peak of up to 50 V. Droplets were generated on-demand either individually or in burst mode with a known total number of droplets.

The paper spray was operated with either pure methanol (Fisher Chemical, USA; 0.2 micron filtered) or an equal volume mix of methanol and chloroform (Fisher Chemicals, USA; Approx. 0.75% ethanol as preservative) delivered at a flow rate of 20 $\mu\text{L min}^{-1}$ using a syringe pump.

2.2 Apparatus

All measurements were carried out using a Q Exactive Focus Orbitrap Mass Spectrometer (ThermoFisher Scientific, USA). The paper spray ion source was constructed in-house to deliver ions to the inlet of the MS through a metal extension loosely affixed to the inlet to act as a funnel. The funnel was observed to increase signal intensity and improve stability, attributed to the increased time over which electrospray droplets could evaporate. The MS was operated in negative polarity mode to detect acids and positive mode to detect the glycols, with typical scan settings of 90–300 m/z , a resolution of 35 000 and maximum ion injection time of 100 ms.

Two different types of paper spray substrate were used in this study: VWR filter paper (Filter Paper, Qualitative, 413) and Whatman chromatography paper (Standard chromatography paper, Thickness: 0.18 mm; Flow Rate: 130 mm/30 min). Triangular substrates were prepared from a 1 cm \times 1 cm square by cutting from the corner to the center to produce isosceles triangles with base 1 cm and height 1 cm, leading to a tip angle of 53°. Other geometries were also sampled, however a rigorous comparison was not performed as previous works have addressed the effects of tip angle.⁵¹

The paper substrate was attached to a stainless-steel alligator clip mounted to a 3D printed enclosure and connected to a high voltage power supply (Stanford Research Systems PS350). The paper substrate was loosely connected to a PEEK solvent

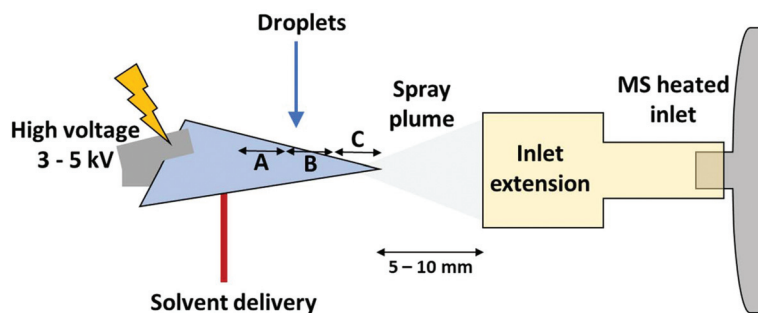


Fig. 1 Schematic configuration of the paper spray ionization source coupled to the mass spectrometer. Droplets are deposited on-demand from a microdispenser above the paper at locations near the solvent delivery tube (position A), towards the tip (position B) and at the tip (position C). The MS inlet extension improves the ion collection efficiency in the absence of heated gases, serving to funnel the ions and aid in evaporation of the electro spray plume. The PS–MS interface is housed within a 3D printed enclosure with the paper protruding into the open lab environment.

delivery tube to receive solvent flow from a 10 mL syringe (Hamilton, USA; Model: GasTight #1010) pushed by a syringe pump (Chemyx Inc., USA; Model: Fusion 100T) operating at $20 \mu\text{L min}^{-1}$. The droplet dispenser was mounted using opto-mechanical components (Thorlabs) and positioned above the paper substrate. A schematic of the PS ionization platform is shown in Fig. 1.

2.3 Droplet paper spray

The basic principles of paper spray have been discussed elsewhere and are recounted only briefly here.⁴⁷ To generate an electro spray from the tip of the paper, a voltage of 3–5 kV was applied to the solvent-soaked substrate. Above a certain voltage threshold, an electro spray plume was emitted from the tip of the paper towards the MS inlet (held at 50 V). Unlike more traditional paper spray implementations, solvent was continuously delivered to the paper allowing the spray to be maintained indefinitely. The tip of the paper was positioned 5–10 mm from the inlet to the MS resulting in a spray plume that expands to the width of the modified inlet region at the inlet (Fig. 1).

Picoliter aqueous droplets containing the sample analyte were deposited onto the paper substrate during paper spray operation. The deposition location was not rigorously measured due to the difficulties associated with imaging the droplets and assessing their trajectories. However, the location was categorized crudely into three regions, indicated in Fig. 1: A – near the solvent delivery site; B – between the solvent delivery site and the tip; C – near the tip. The spacing between these regions was approximately 1 mm. Once deposited on the surface, droplets were solubilized by the solvent and the solution flowed towards the tip of the paper, eventually being sprayed in the plume resulting in sample ionization. Depending on deposition location and analyte mass in the sample, the material was present in the spray for seconds to minutes. Ions from the spray were continuously sampled by the MS and a clear increase in intensity corresponding to analyte peaks was observed following deposition, followed by a decay as the material was depleted. This approach leads to two

main advantages – firstly, the distinction between background and noise peaks in the spectrum compared to analyte peaks is very clear and secondly, many samples can be analyzed and compared in quick succession without modification of the ionization assembly.

2.4 Data processing

Experimental mass spectra were initially analyzed using Xcalibur 4.1 software (ThermoFisher Scientific) and chromatograms of relevant peaks were exported for further analysis.

3. Results and discussion

To explore the nature of the paper spray method as applied to analyte contained within single picolitre droplets, we explore the response to a series of single and mixed analyte samples. We first demonstrate sensitivity of PS–MS to a range of compounds relevant for the study of oxidized organic material present in atmospheric aerosol and explore the reproducibility. We go on to assess the quantitative nature of the response of signal intensity to the mass of analyte contained within the deposited droplets and the relative signal arising from mixed analyte samples.

3.1 Compositional analysis of single analyte droplets

3.1.1 Chemical identification. Individual picoliter droplets produced from a 1 g L^{-1} solution of citric acid (CA) were deposited on the paper spray substrate and the resulting ions were sampled by PS–MS. Based on previous work, the droplets produced using the microdispenser were on the order of $50 \mu\text{m}$ in diameter, leading to a total mass of citric acid in a single droplet of $\sim 65 \text{ pg}$.⁵² Following deposition, the signal in the mass spectrum corresponding to the single deprotonated citric acid molecule (m/z 191.02) increased significantly and decayed over subsequent seconds. A chromatogram of several droplet deposition events is shown in Fig. 2A, with each peak in the sequence arising from a single droplet deposited on the paper. With each droplet giving rise to a peak that persists for

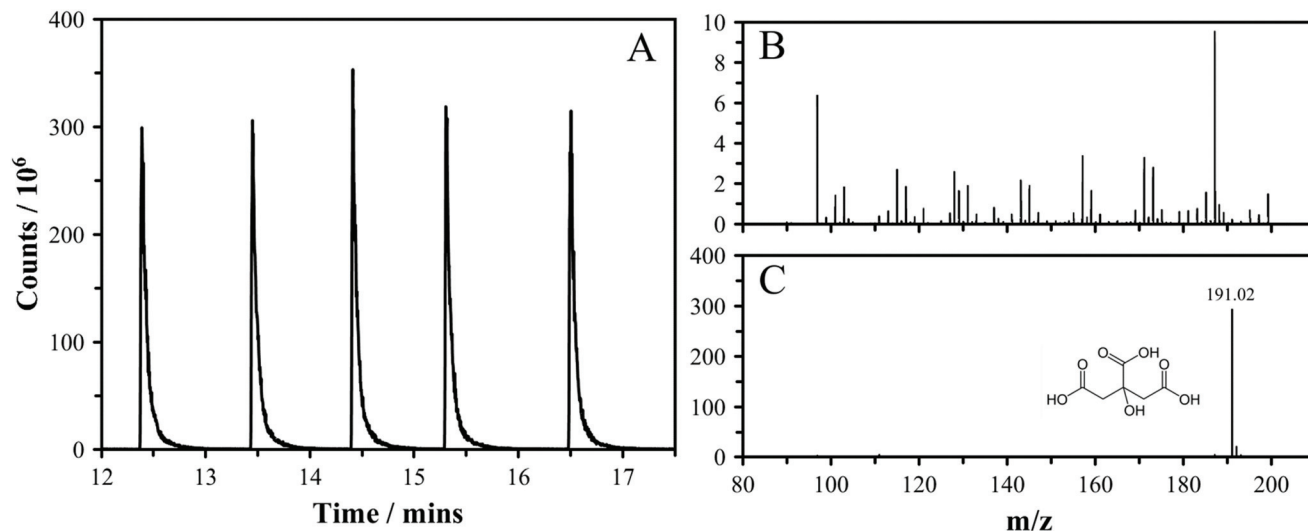


Fig. 2 (A) A sequence of single five citric acid (CA) solution droplets with a diameter of $\sim 50 \mu\text{m}$ and a concentration of 1 g L^{-1} (65 pg of CA) were sampled by PS-MS. The counts correspond to the intensity of the molecular ion peak for citric acid ($\text{C}_6\text{H}_7\text{O}_7^+$). (B) The background mass spectrum measured in the paper spray. (C) The mass spectrum corresponding to the peak intensity from a single droplet of citric acid. Note that the axis range is 40x larger than in Fig. 2B.

around 0.2 min , and a solvent flow rate of $20 \mu\text{L min}^{-1}$, we can estimate the average concentration of analyte in the electro-spraying solution to be on the order of $10 \text{ pg } \mu\text{L}^{-1}$.

Fig. 2B shows the mass spectrum prior to deposition of a droplet and Fig. 2C shows the mass spectrum at the peak of signal arising from the droplet. While there is intensity in background peaks arising solely from the paper spray, the spectrum shows a clear contribution from the droplet following deposition. The ability to unambiguously identify peaks arising from our sample makes this technique useful for characterizing samples of unknown composition. To explore the breadth of application of the technique for the chemical identification of atmospherically relevant species, we measured mass spectra for a series of polyethylene glycol droplets (tetra, penta and hexa-ethylene glycols), long-chain fatty acids (oleic and elaidic acid) and a series of dicarboxylic acids (glutaric, succinic and adipic acid). We have limited our exploration to oxidized molecules as these form the majority of secondary organic aerosol species in the atmosphere.⁵³ Fig. 3 clearly shows that the droplet PS-MS method is capable of identification of these dicarboxylic acids (Fig. 3A), glycols (Fig. 3B) and fatty acids (Fig. 3C). These molecules span a range of solubility (in water) and molecular mass. For the acids, the major ion is the singly deprotonated molecular ion, while for the glycols (measured in positive mode) the major ions were the sodium and ammonium adducts with the parent molecule, and the singly protonated ion.⁵⁴ These results demonstrate that there is broad applicability of the technique to sample oxygenated species representative of atmospheric secondary organic aerosol material.

3.1.2 Reproducibility. We have shown that qualitative identification of a wide range of analytes in picoliter droplets is possible using the PS-MS method. However, in order to

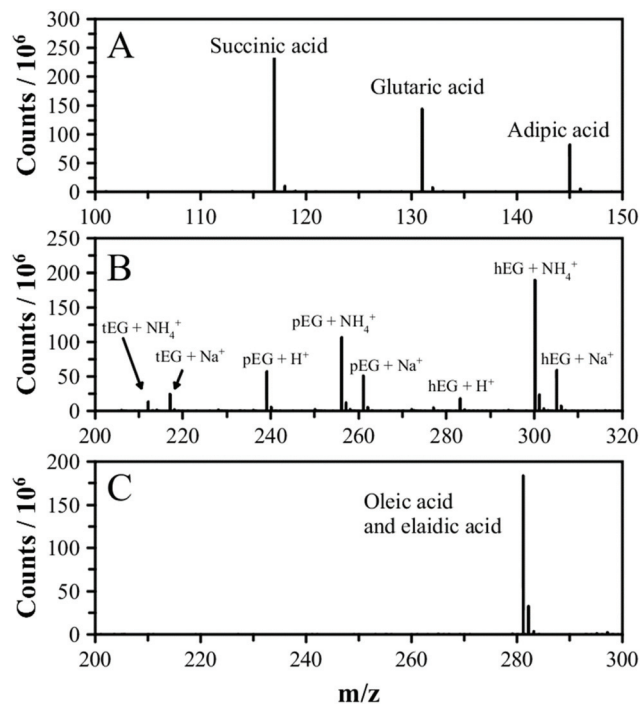


Fig. 3 Mass spectra obtained for single droplets deposited on the paper for equimolar mixtures of dicarboxylic acids (A), polyethylene glycols (t = tetra, p = penta, h = hexa, EG = ethylene glycol) (B) and oleic acid (and its configurational isomer elaidic acid) (C). The acids were sampled in negative ionization mode, while the glycols were sampled in positive mode and the spectra shows peaks corresponding to $M + \text{H}^+$, $M + \text{NH}_4^+$ and $M + \text{Na}^+$.

apply it to measuring reaction rates and chemical abundances, the method must also produce reproducible data that quantitatively reflects the sample composition.

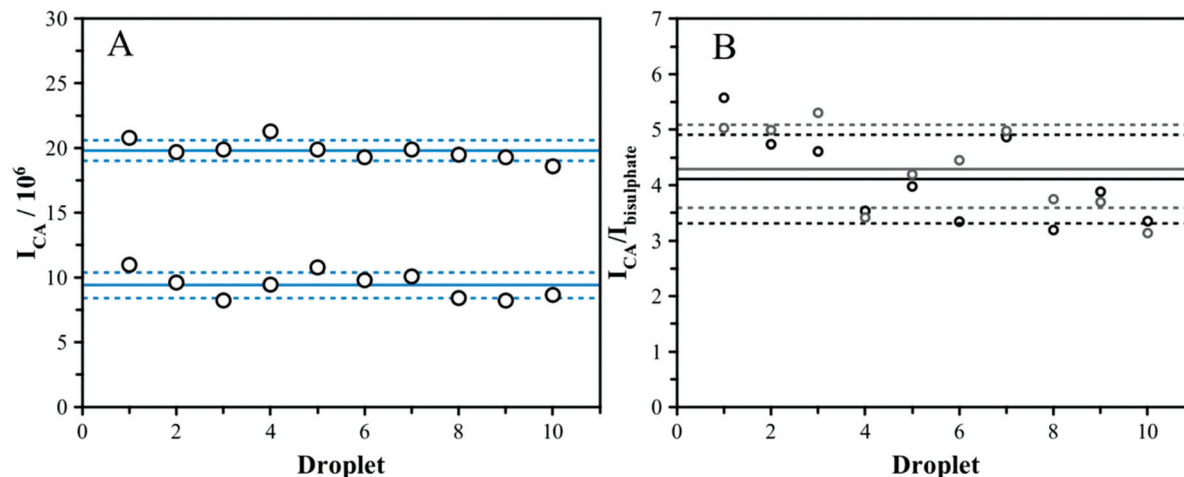


Fig. 4 (A) For the citric acid solution droplets as Fig. 2, the peak area corresponding to the molecular ion was found, shown here for each individual droplet in a sequence of 10. Two datasets for the same solution, and the differences can be attributed to the variations in the system on an experiment by experiment basis, as discussed in the text. The solid blue lines shows the average while the dash lines represent an uncertainty range of one standard deviation. (B) The citric acid chromatograms were ratioed against the bisulphate (HSO_4^-) chromatogram, a consistent background peak in the paper spray. The average peak area ratio for the two experiments converge, although the signal variability increases due to the variability of the relatively low intensity bisulphate signal. The solid lines show the average while the dash lines show the new standard deviation range associated with the ratio.

The chromatogram signal corresponding to a single droplet may be integrated to determine the area under the curve, hereby referred to as the peak area or I_x , where X reflects the analyte of interest. We will assess the assumption that peak area is proportional to the mass of analyte sampled. For a series of droplets where the mass of analyte is approximately constant, we observed reproducibility within a few percent between individual droplets. Fig. 4A shows representative data for the peak area for two separate experiments with 10 droplets of a 1 g L^{-1} citric acid solution collected sequentially. In these cases, the standard deviation is around 10% of the mean, with no systematic trend. This reproducibility was observed in the majority of experiments.

It should be clear from Fig. 4 that although there is good reproducibility over the course of a measurement, there is little reproducibility when comparing the same concentration on different days. Fig. 4A shows two sets of data, collected with the same 1 g L^{-1} CA sample solution and droplet dispenser pulse settings, that exhibit a factor of two difference in the average peak intensity. There are several factors that might be responsible for this:

Deposition location. The deposition location may differ when the experiment is set up on successive occasions. Fig. S1† shows the chromatogram for individual droplets deposited at three locations on the paper (defined as A, B and C in Fig. 1). In the case when the dispenser is placed very close to the tip (C), we observe a very sharp and narrow peak. This is due to the small surface area and volume of solvent in which the analyte can dissolve, leading to a high effective concentration in the spray. However, with the dispenser positioned far from the tip (position A), we observe a slow rise in signal and broad peaks that persist for longer. The low peak intensity and long

duration over which the analyte may become absorbed to the porous paper might limit the sensitivity in this configuration. Position B (between positions A and C) leads to the largest peak area ($\sim 2\times$ the area for the peak at position C), while the peak at position C shows the smallest area. It is clear that a consistent deposition location (position B is considered the most suitable throughout study) is vital for gaining consistent signal in PS-MS.

Spray characteristics. Although in principle the spray can be maintained indefinitely with continuous supply of solvent, in reality it must be restarted every 4–5 hours to refill the solvent syringe. Typically, the measured signal is consistent across this time period. However, when the spray stops and is restarted, even with the same voltage settings, the signal intensity can be quite different. This is likely due to the changes in microscopic structure of the paper and the protrusions that are actively producing electrosprays.⁴⁷ This sensitivity to changes is even more pronounced when the paper substrate is changed, as the microscopic structure will be totally transformed.

Droplet size. Each time the droplet dispenser is loaded with sample solution, the capillary forces that pull the liquid to the tip can change marginally. This can result in differently sized droplets being produced, which can lead to inter-experimental variability. Although the micro dispensers have been shown to produce consistently sized droplets within a few % of mean diameter, this marginal change in size could lead to a large variation in the mass due to the cubic relationship between size and mass and account for some of the uncertainty.

The factors above that affect the reproducibility can be mitigated by avoiding any changes to the setup over the course of an experiment (constant spray and unchanged dispenser location). In addition, an internal standard can be used that

gives an indication of the efficiency of the spray. In Fig. 4B, the peak at m/z 96.96, a consistent feature in the paper spray plume and likely arising from bisulfate (HSO_4^-), is used to normalize the citric acid data from Fig. 4A. The data becomes more scattered, as now the variability in two peaks contributes. However, the mean values for these data are consistent, within a few percent. This suggests that the differences in the signal intensity between experiments arise from the variability in dispenser position as well as spray characteristics and may be accounted for by normalizing to a peak that is representative of the spray efficiency. Additionally, ensuring that the factors that give rise to variability are constrained will improve the reproducibility of results between experiments.

3.1.3 Quantification. In order to assess the quantitative nature of the method, and in light of the signal reproducibility observations when aspects of the setup are changed, we used the droplet dispenser in burst mode to vary the analyte mass and explore the response in the MS. While this is not directly equivalent to a large or more highly concentrated single droplet, it provides an effective means of quickly varying the analyte mass while maintaining the experimental configuration in a fixed state. Droplets were generated at up to 200 per burst, allowing the analyte mass to span over two orders of magnitude. Experiments were performed using a 0.1 g L^{-1} citric acid solution and repeated several times over different days. The results are shown in Fig. 5 using chloroform/methanol as the spray solvent. We observe clear variability on an experiment-to-experiment basis, as already discussed. However, within a single experiment, we observe a linear

relationship between the signal intensity and analyte mass (calculated assuming a droplet diameter of $50 \mu\text{m}$). The slope of the dependence varies, but in all cases the R^2 is greater than 0.9 indicating that the response of the system is linear to analyte mass over the range explored here, from around 50 pg to 1.3 ng . Over a narrow range of mass, shown inset in Fig. 5, the linearity is excellent, with an R -squared of >0.99 . The full mass range explored here is equivalent to a particle of pure CA with diameter from $1.4 \mu\text{m}$ to $4.4 \mu\text{m}$. The limit of detection, estimated by the analyte mass that gives rise to a signal to noise of $10:1$, is on the order of 0.5 pg , equivalent to a pure CA particle diameter of $0.3 \mu\text{m}$.

Earlier measurements with pure methanol as the spray solvent show linearity only over a narrower range of mass, with clear curvature as low analyte mass loadings are approached (Fig. S2†). The reason for this is unclear but may arise due to the voltage required to generate a stable spray. For the mixed solvent, voltages of $>4 \text{ kV}$ were used, while for pure methanol, a spray was typically stable at $3.2\text{--}3.5 \text{ kV}$. The greater electric field required to generate stable electrospray from the chloroform/methanol solvent might have improved ion production at high analyte concentrations and make the measurement less susceptible to charge limitations.⁵⁵

In the case of citric acid, these results demonstrate that for a single component analyte sampled under consistent conditions, the signal is both reproducible and linear. These factors are vital for applications of the PS-MS in the analysis of compositional changes in levitated droplets. However, in most measurements, droplets will not contain just one analyte and instead consist of two or more (and up to thousands for ambient samples) different chemical species. Such analysis can be simplified by considering the peak area of an analyte relative to other analytes within the sample to normalize the data. However, relative ionization efficiencies of these compounds must be known or measured in order the gain quantitative information from these data. Here, we will focus our discussion on a binary system to assess the key features of the droplet PS-MS method when applied to a droplets containing mixed analytes.

3.2 Compositional analysis of binary analyte droplets

3.2.1 Relative intensity and ionization efficiency. When dealing with droplets containing mixed analytes, we can consider the ratio of the intensity of analyte peaks. The mole fraction in a binary droplet (in this case consisting of maleic acid (MA) and citric acid (CA)) can be written as a function of the peak area in the mass chromatogram according to:

$$x_{\text{MA}} = \frac{\gamma I_{\text{MA}}}{\gamma I_{\text{MA}} + I_{\text{CA}}} \quad (1)$$

where I_{MA} and I_{CA} are the peak areas of the analytes in the chromatogram. γ denotes the relative ionization efficiency of maleic acid to citric acid, according to:

$$\gamma = \frac{I_{\text{CA}} n_{\text{MA}}}{I_{\text{MA}} n_{\text{CA}}} \quad (2)$$

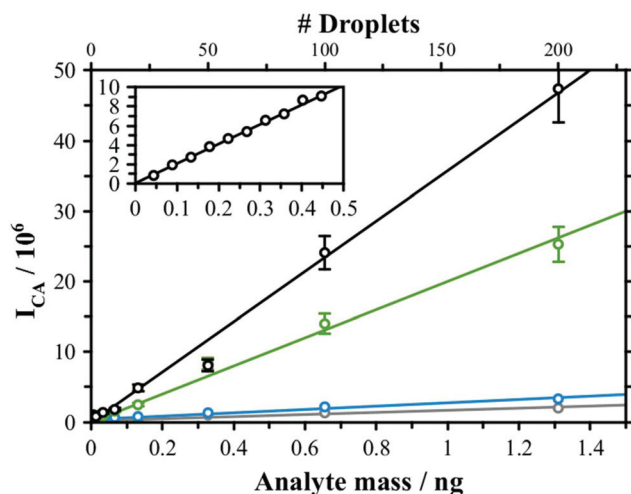


Fig. 5 The integrated peak area of citric acid sampled from droplets as a function of analyte mass increases linearly over a mass range of at least two orders of magnitude. The analyte mass was varied by deposition of between 1 and 200 droplets of a 0.01 g L^{-1} citric acid solution in burst method, as discussed in the text. Each line represents data collected during different experiments on different days using the same solution. The inter-experimental variability is discussed in the text. (Inset) Low mass range analysis with higher resolution also shows linearity.

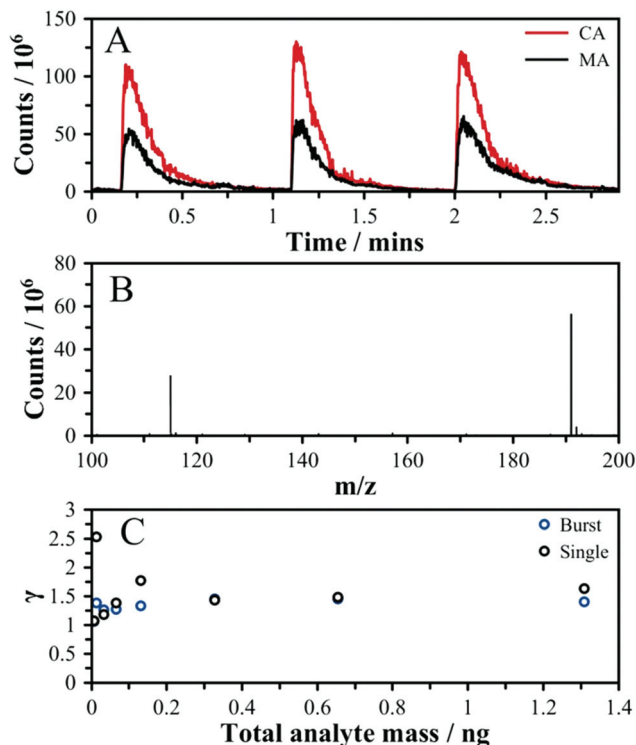


Fig. 6 (A) Chromatogram of peaks corresponding to single droplets containing citric acid (red) and maleic acid (black) in an equimolar mixture. (B) Mass spectrum showing contribution from citric acid (191.02) and maleic acid (115.00) molecular ions. (C) Ionization efficiency (as defined in the text) determined for maleic acid and citric acid as a function of total analyte mass for experiments in burst mode and single droplet mode. Both methods exhibit a trend towards an ionization efficiency of ~ 1.5 with total analyte mass > 0.1 ng.

where n_{MA} and n_{CA} are the molar amounts of maleic acid and citric acid in the sample droplet. For an equimolar mixture of MA and CA, the mole ratio is equal to one, and the ionization efficiency is determined directly from the relative intensity of the signals from each analyte. The chromatogram for MA and CA in a droplet comprised of an equimolar mixture is shown in Fig. 6A and a representative mass spectrum for this composition is shown in Fig. 6B. The relative ionization efficiency is determined to be 1.89. However, there is significant variability in this value, especially at low analyte mass. At high analyte mass, the ionization ratio tends towards a consistent value. Fig. 6C compares the ionization efficiency for equimolar mixtures of citric acid and maleic acid for increasing analyte mass. These measurements were performed using both burst mode and single droplets with increasing solute concentration. For the single droplet measurements, there is large variability in the ratio until the analyte total mass is greater than around 0.1 ng, while for the burst mode the variability is much smaller. The comparison of these datasets indicates once again that the deposition location is a key factor in the reproducibility of data. In burst mode, the droplet dispenser location is fixed, and all droplets are deposited at the same location. In single droplet mode, the dispenser was removed and replaced each time with a new sample solution, introducing some variability.

3.2.2 Evaluating the relative abundance. To explore how the signal intensity varies when the mixing ratio of analytes changes, we performed a series of measurements on single droplets of CA and MA mixture from solutions spanning a range of MA mole fractions, from $x_{\text{MA}} = 0.02$ to $x_{\text{MA}} = 0.94$. This is shown in Fig. 7A for single droplets generated from

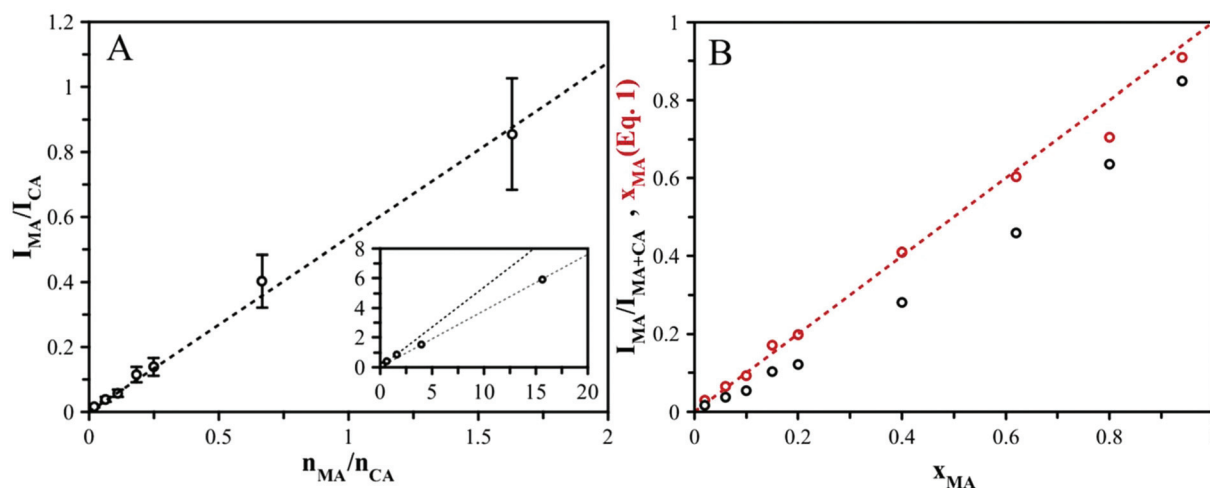


Fig. 7 (A) The ratio of maleic acid (MA) to citric acid (CA) peak areas is shown as a function of the molar ratio in the droplet. A linear trend with a slope of 0.54 is observed up to $n_{\text{MA}}/n_{\text{CA}} \approx 2$, but beyond that some deviation is observed (inset: black dash line shows the fit up to $n_{\text{MA}}/n_{\text{CA}} \approx 2$ versus a linear fit to all the data shown as a gray dash line). Taking a linear fit to the data up to $n_{\text{MA}}/n_{\text{CA}} \approx 2$, an ionization efficiency of 1.84 is determined. (B) The peak area of MA as a fraction of the total peak area from CA and MS is shown as a function of mole fraction of MA in the droplet (black points). The curvature arises due to the ionization efficiency effects. Accounting for the ionization efficiency using the slope of the data in (A) and eqn (3), the mole fraction can be estimated (red points) using eqn (1). The 1 : 1 line is shown as a red dash.

1–20 g L⁻¹ total analyte concentration sample solutions (an average across experiments using different mass concentrations is shown). The points show the average of three repeats over different days, and each repeat took the average of 10 individual sequential droplets per data point. The error bars reflect the standard deviation of 10% representative of the variability on a droplet-by-droplet basis.

The slope of the peak area ratio against the molar ratio defines the ionization efficiency, according to:

$$\frac{I_{\text{MA}}}{I_{\text{CA}}} = \frac{1}{\gamma} \frac{n_{\text{MA}}}{n_{\text{CA}}} \quad (3)$$

For molar ratios up to ~ 2 (*i.e.* 2 molecules of MA to every 1 of CA), the data define a straight line with an R^2 of 0.994, a slope of 0.54 and a standard deviation in the slope of 0.02. This indicates that the relative ionization efficiency is constant over this range with a value of 1.85, in agreement with the determined value from the equimolar mixture in section 3.2.1. When the full range of data are included in the fit, there is some curvature and a straight line is no longer a good representation of the whole data set shown in the inset of Fig. 7A. A straight line fit through all the data points varies significantly from the straight line defining just the lower molar ratio points.

The MA peak area as a function of the total peak area is shown in Fig. 7B and exhibits a curvature as the data approach the limiting points (0,0 and 1,1). This curvature is due to the difference in ionization efficiencies of analytes and accounting for the relative ionization efficiency, *via* eqn (1), allows us to calculate the expected mole fraction from the intensity. These data exhibit agreement to a 1 : 1 line, indicating that the mole fraction is determined accurately. The points at higher mole fraction also agree well with the 1 : 1 line, even though the relative ionization efficiency predicted by these data is much larger. This is a consequence of the choice of parameters and arises due to the much smaller dependence of the peak area ratio on the ionization efficiency when at the extreme ends of the mole fraction range.

4. Conclusions

We have demonstrated several key features of the droplet PS-MS platform that will guide future application of the method for sampling levitated droplets. Firstly, the sensitivity of the method to oxygenated organic compounds in both positive and negative ion modes ensures that compounds of atmospheric interest and the products from atmospherically relevant reactions (such as ozonolysis and OH-initiated oxidation) can be effectively analyzed using this method. Secondly, we demonstrate high droplet-by-droplet reproducibility (within 10%) and identified key experimental factors that must be constrained to achieve this. When coupling the PS-MS ionization source to an LQ-EDB, the sequential sampling of individual droplets may occur over many minutes or even hours, and it is imperative that the system response over that time be well

understood. We have further shown that both internal and external standards can mitigate some variability in the signal. Finally, we have shown that both the absolute signal and the relative signals are effective indicators of abundance, with linearity observed over the entire mass range relevant for levitation studies and over a broad range of composition. Further improvements to the platform may be achieved through the use of different solvents, paper substrate composition and experimental geometry to improve sensitivity or reproducibility.

Although further work with quantitative measures of suspended droplet size are required to fully characterize the technique, we have shown through these measurements that the droplet PS-MS platform will be an effective tool for compositional analysis of levitated picoliter droplets and quantification of changes in their composition due to evaporation or chemical reaction. The coupling of PS-MS with an a linear-quadrupole electrodynamic balance (LQ-EDB) will facilitate experimental interrogations of the evolving chemical composition of levitated droplet samples and allow physical and optical properties to be measured as a function of composition.⁵⁶ For this, samples will be drawn from solutions of model atmospheric compounds or resolubilized laboratory-generated of ambient aerosol material and droplets will be introduced into the LQ-EDB using the microdroplet dispensers described in this work. Direct sampling of aerosol by coalescence of laboratory-generated aerosol into a levitated collection droplet may also be possible.⁵⁷ These measurements will be used to characterize the effects of evolving composition due to various atmospheric processes, such as heterogeneous reactions and photochemistry experienced by aerosol in the environment,^{6,25} in order to provide a compositionally-resolved understanding of aerosol properties and processes.

Conflicts of interest

There are no conflicts of interest to declare.

Acknowledgements

We thank the American Society for Mass Spectrometry (ASMS) for support of this work through the ASMS 2019 Research Award. We thank Dr Kevin Wilson and Dr Megan Willis (Lawrence Berkeley National Laboratory) for helpful discussions.

References

- 1 C. R. Ruehl, J. F. Davies and K. R. Wilson, *Science*, 2016, **351**, 1447–1450.
- 2 M. C. Facchini, M. Mircea, S. Fuzzi and R. J. Charlson, *Nature*, 1999, **401**, 257.

- 3 U. Lohmann, K. Broekhuizen, R. Leitch, N. Shantz and J. Abbatt, *Geophys. Res. Lett.*, 2004, **31**, L05108.
- 4 A. T. Lambe, C. D. Cappa, P. Massoli, T. B. Onasch, S. D. Forestieri, A. Martiner, T. M. J. Cummings, D. R. Croasdale, W. H. Brune, D. R. Worsnop and P. Davidovits, *Environ. Sci. Technol.*, 2013, **47**, 6349–6357.
- 5 T. Moise, J. M. Flores and Y. Rudich, *Chem. Rev.*, 2015, **115**, 4400–4439.
- 6 C. George, M. Ammann, B. D'Anna, D. J. Donaldson and S. A. Nizkorodov, *Chem. Rev.*, 2015, **115**, 4218–4258.
- 7 R. C. Chapleski, Y. Zhang, D. Troya and J. R. Morris, *Chem. Soc. Rev.*, 2016, **45**, 3731–3746.
- 8 M. Jang, B. Carroll, B. Chandramouli and R. M. Kamens, *Environ. Sci. Technol.*, 2003, **37**, 3828–3837.
- 9 U. Pöschl, *Angew. Chem., Int. Ed.*, 2005, **44**, 7520–7540.
- 10 M. Shiraiwa, K. Selzle and U. Pöschl, *Free Radic. Res.*, 2012, **46**, 927–939.
- 11 G. Isaacman-VanWertz, P. Massoli, R. O'Brien, C. Lim, J. Franklin, J. Moss, J. Hunter, J. Nowak, M. Canagaratna, P. Misztal, C. Arata, J. Roscioli, S. Herndon, T. Onasch, A. Lambe, J. Jayne, L. Su, D. Knopf, A. Goldstein, D. Worsnop and J. Kroll, *Nat. Chem.*, 2017, **10**, 462–468.
- 12 Q. Zhang, J. L. Jimenez, M. R. Canagaratna, J. D. Allan, H. Coe, I. Ulbrich, M. R. Alfarra, A. Takami, A. M. Middlebrook, Y. L. Sun, K. Dzepina, E. Dunlea, K. Docherty, P. F. DeCarlo, D. Salcedo, T. Onasch, J. T. Jayne, T. Miyoshi, A. Shimono, S. Hatakeyama, N. Takegawa, Y. Kondo, J. Schneider, F. Drewnick, S. Borrmann, S. Weimer, K. Demerjian, P. Williams, K. Bower, R. Bahreini, L. Cottrell, R. J. Griffin, J. Rautiainen, J. Y. Sun, Y. M. Zhang and D. R. Worsnop, *Geophys. Res. Lett.*, 2007, **34**, L13801.
- 13 J. T. Jayne, D. C. Leard, X. Zhang, P. Davidovits, K. A. Smith, C. E. Kolb and D. R. Worsnop, *Aerosol Sci. Technol.*, 2000, **33**, 49–79.
- 14 P. F. DeCarlo, J. R. Kimmel, A. Trimborn, M. J. Northway, J. T. Jayne, A. C. Aiken, M. Gonin, K. Fuhrer, T. Horvath, K. S. Docherty, D. R. Worsnop and J. L. Jimenez, *Anal. Chem.*, 2006, **78**, 8281–8289.
- 15 J. Laskin, A. Laskin and S. A. Nizkorodov, *Anal. Chem.*, 2018, **90**, 166–189.
- 16 J. Laskin, A. Laskin and S. A. Nizkorodov, *Anal. Chem.*, 2018, **90**, 166–189.
- 17 J. D. Hearn and G. D. Smith, *Anal. Chem.*, 2004, **76**, 2820–2826.
- 18 F. D. Lopez-Hilfiker, C. Mohr, M. Ehn, F. Rubach, E. Kleist, J. Wildt, Th. F. Mentel, A. Lutz, M. Hallquist, D. Worsnop and J. A. Thornton, *Atmos. Meas. Tech.*, 2014, **7**, 983–1001.
- 19 T. Nah, M. Chan, S. R. Leone and K. R. Wilson, *Anal. Chem.*, 2013, **85**, 2087–2095.
- 20 K. T. Upton, K. A. Schilling and J. L. Beauchamp, *Anal. Methods*, 2017, **9**, 5065–5074.
- 21 J. H. Gross, *Anal. Bioanal. Chem.*, 2014, **406**, 63–80.
- 22 M. Brüggemann, E. Karu, T. Stelzer and T. Hoffmann, *Environ. Sci. Technol.*, 2015, **49**, 5571–5578.
- 23 A. J. Horan, M. J. Apsokardu and M. V. Johnston, *Anal. Chem.*, 2016, **89**, 1059–1062.
- 24 J. Smith, J. Kroll, C. Cappa, D. L. Che, C. L. Liu, M. Ahmed, S. R. Leone, D. R. Worsnop and K. Wilson, *Atmos. Chem. Phys.*, 2009, **9**, 3945–3981.
- 25 B. R. Bzdek and J. P. Reid, *J. Chem. Phys.*, 2017, **147**, 220901.
- 26 U. K. Krieger, J. P. Reid and U. K. Krieger, *Chem. Soc. Rev.*, 2012, **41**, 6631–6662.
- 27 M. N. Chan, M. Y. Choi, N. L. Ng and C. K. Chan, *Environ. Sci. Technol.*, 2005, **39**, 1555–1562.
- 28 J. F. Davies, A. E. Haddrell, A. M. J. Rickards and J. P. Reid, *Anal. Chem.*, 2013, **85**, 5819–5826.
- 29 C. Cai, D. J. Stewart, J. P. Reid, Y. Zhang, P. Ohm, C. S. Dutcher and S. L. Clegg, *J. Phys. Chem. A*, 2014, **119**, 704–718.
- 30 N. A. Hosny, C. Fitzgerald, C. Tong, M. Kalberer, M. K. Kuimova and F. D. Pope, *Faraday Discuss.*, 2013, **165**, 343–356.
- 31 H. C. Price, B. J. Murray, J. Mattsson, D. O'Sullivan, T. W. Wilson, K. J. Baustian and L. G. Benning, *Atmos. Chem. Phys.*, 2014, **14**, 3817–3830.
- 32 B. R. Bzdek, R. M. Power, S. H. Simpson, J. P. Reid and C. P. Royall, *Chem. Sci.*, 2016, **7**, 274–285.
- 33 R. M. Power, S. H. Simpson, J. P. Reid and A. J. Hudson, *Chem. Sci.*, 2013, **4**, 2597–2604.
- 34 M. I. Cotterell, R. E. Willoughby, B. R. Bzdek, A. J. Orr-Ewing and J. P. Reid, *Atmos. Chem. Phys.*, 2017, **17**, 9837–9851.
- 35 K. Gorkowski, H. Beydoun, M. Aboff, J. S. Walker, J. P. Reid and R. C. Sullivan, *Aerosol Sci. Technol.*, 2016, **50**, 1–15.
- 36 D. L. Bones, J. P. Reid, D. M. Lienhard and U. K. Krieger, *Proc. Natl. Acad. Sci. U. S. A.*, 2012, **109**, 11613–11618.
- 37 P. J. Tracey, B. S. Vaughn, B. J. Roberts, B. L. J. Poad and A. J. Trevitt, *Anal. Chem.*, 2014, **86**, 2895–2899.
- 38 Y. Huang, K. M. Barraza, C. M. Kenseth, R. Zhao, C. Wang, J. L. Beauchamp and J. H. Seinfeld, *J. Phys. Chem. A*, 2018, **122**, 6445–6456.
- 39 C. Warschat, A. Stindt, U. Panne and J. Riedel, *Anal. Chem.*, 2015, **87**, 8323–8327.
- 40 M. I. Jacobs, J. F. Davies, L. Lee, R. D. Davis, F. Houle and K. R. Wilson, *Anal. Chem.*, 2017, **89**, 12511–12519.
- 41 A. W. Birdsall, U. K. Krieger and F. N. Keutsch, *Atmos. Meas. Tech.*, 2018, **115194**, 33–47.
- 42 A. W. Birdsall, J. C. Hensley, P. S. Kotowitz, A. J. Huisman and F. N. Keutsch, *Atmos. Chem. Phys.*, 2019, **19**, 14195–14209.
- 43 M. I. Jacobs, J. F. Davies, L. Lee, R. D. Davis, F. Houle and K. R. Wilson, *Anal. Chem.*, 2017, **89**, 12511–12519.
- 44 H. Wang, J. Liu, R. G. Cooks and Z. Ouyang, *Angew. Chem., Int. Ed.*, 2010, **49**, 877–880.
- 45 J. Liu, H. Wang, N. E. Manicke, J.-M. Lin, R. G. Cooks and Z. Ouyang, *Anal. Chem.*, 2010, **82**, 2463–2471.
- 46 N. Riboni, A. Quaranta, H. V. Motwani, N. Österlund, A. Gräslund, F. Bianchi and L. L. Ilag, *Sci. Rep.*, 2019, **9**, 1–12.

- 47 R. D. Espy, A. R. Muliadi, Z. Ouyang and R. G. Cooks, *Int. J. Mass Spectrom.*, 2012, **325–327**, 167–171.
- 48 S. Banerjee and S. Mazumdar, *Int. J. Anal. Chem.*, 2012, **2012**, 1–40.
- 49 D. Kim, U. H. Yim, B. Kim, S. Cha and S. Kim, *Anal. Chem.*, 2017, **89**, 9056–9061.
- 50 J. F. Davies, *Aerosol Sci. Technol.*, 2019, **53**, 309–320.
- 51 Q. Yang, H. Wang, J. D. Maas, W. J. Chappell, N. E. Manicke, R. G. Cooks and Z. Ouyang, *Int. J. Mass Spectrom.*, 2012, **312**, 201–207.
- 52 J. F. Davies, A. E. Haddrell and J. P. Reid, *Aerosol Sci. Technol.*, 2011, **46**, 666–677.
- 53 J. L. Jimenez, M. R. Canagaratna, N. M. Donahue, A. S. H. Prevot, Q. Zhang, J. H. Kroll, P. F. DeCarlo, J. D. Allan, H. Coe, N. L. Ng, A. C. Aiken, K. S. Docherty, I. M. Ulbrich, A. P. Grieshop, A. L. Robinson, J. Duplissy, J. D. Smith, K. R. Wilson, V. A. Lanz, C. Hueglin, Y. L. Sun, J. Tian, A. Laaksonen, T. Raatikainen, J. Rautiainen, P. Vaattovaara, M. Ehn, M. Kulmala, J. M. Tomlinson, D. R. Collins, M. J. Cubison, E. J. Dunlea, J. A. Huffman, T. B. Onasch, M. R. Alfarra, P. I. Williams, K. Bower, Y. Kondo, J. Schneider, F. Drewnick, S. Borrmann, S. Weimer, K. Demerjian, D. Salcedo, L. Cottrell, R. Griffin, A. Takami, T. Miyoshi, S. Hatakeyama, A. Shimono, J. Y. Sun, Y. M. Zhang, K. Dzepina, J. R. Kimmel, D. Sueper, J. T. Jayne, S. C. Herndon, A. M. Trimborn, L. R. Williams, E. C. Wood, A. M. Middlebrook, C. E. Kolb, U. Baltensperger and D. R. Worsnop, *Science*, 2009, **326**, 1525–1529.
- 54 A. Krueve and K. Kaupmees, *J. Am. Soc. Mass Spectrom.*, 2017, **28**, 887–894.
- 55 K. Tang, J. S. Page and R. D. Smith, *J. Am. Soc. Mass Spectrom.*, 2004, **15**, 1416–1423.
- 56 C. L. Price, A. Bain, B. J. Wallace, T. C. Preston and J. F. Davies, *J. Phys. Chem. A*, 2020, DOI: 10.1021/acs.jpca.9b10748.
- 57 A. E. Haddrell, R. E. H. Miles, B. R. Bzdek, J. P. Reid, R. J. Hopkins and J. S. Walker, *Anal. Chem.*, 2017, **89**, 2345–2352.